MULTISCALE MODEL. SIMUL.
Vol. 17, No. 3, pp. 973–995

RASTER GRID PATHOLOGY AND THE CURE*

ALBERT FANNJIANG†

Abstract. Blind ptychography is a phase retrieval method using multiple coded diffraction patterns from different, overlapping parts of the unknown extended object illuminated with an unknown window function. The window function is also known as the probe in the optics literature. As such blind ptychography is an inverse problem of simultaneous recovery of the object and the window function given the intensities of the windowed Fourier transform and has a multiscale set-up in which the probe has an intermediate scale between the pixel scale and the macroscale of the extended object. The uniqueness problem for blind ptychography is analyzed rigorously for the raster scan (of a constant step size τ) and its perturbations. The block phases are shown to form an arithmetic progression and the complete characterization of the raster scan ambiguities is given, including, first, the periodic raster grid pathology of degrees of freedom proportional to τ^2, and, second, a nonperiodic, arithmetically progressing phase shift from block to block. Finally, irregularly perturbed raster scans are shown to remove all ambiguities other than the inherent ambiguities of the scaling factor and the affine phase factor under general requirements, including roughly the minimum overlap ratio 50%.

Key words. blind ptychography, phase retrieval, raster grid pathology, affine phase ambiguity, windowed Fourier transform

AMS subject classifications. 42B, 65T

DOI. 10.1137/18M1227354

1. Introduction.

In the last decade, ptychography has made rapid technological advances and developed into a powerful lensless coherent imaging method [18, 36, 40]. Ptychography collects the diffraction patterns from overlapping illuminations of various parts of the unknown object using a localized coherent source (the probe) [27, 30, 31] and builds on the advances in synthetic aperture methods to extend phase retrieval to unlimited objects and enhance imaging resolution [5, 19, 25, 26, 29] (Figure 1(a)). Blind ptychography goes a step further and seeks to reconstruct both the unknown object and the unknown probe simultaneously [28, 35].

Mathematically, blind ptychography is an inverse problem of simultaneous recovery of the object and the window function (the probe) given the intensities of the windowed Fourier transform (coded diffraction patterns) as the data. In ptychography, the window function has an intermediate scale between the pixel scale and the macroscale of the extended object.

The performance of ptychography depends on factors such as the type of illumination and the measurement scheme, including the amounts of overlap and probe positions. For example, the use of randomly structured illuminations can improve ptychographic reconstruction over that with regular illuminations [3, 7, 8, 10, 11, 16, 21, 29, 32, 33, 34, 38, 39]. Experiments suggest an overlap ratio of at least 50%, typically 60%–70% between adjacent illuminations for blind ptychography [2, 22]. Optimizing the scan pattern can significantly improve the performance of ptychography and is an important part of the experimental design.

*Received by the editors November 19, 2018; accepted for publication (in revised form) June 17, 2019; published electronically August 1, 2019.
https://doi.org/10.1137/18M1227354
Funding: This work was supported by the National Science Foundation under grant DMS-1413373.
†Department of Mathematics, University of California, Davis, CA 95616 (fannjiang@math.ucdavis.edu).

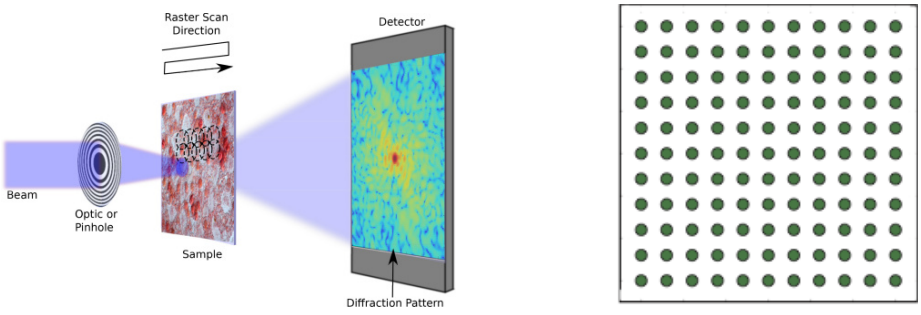

(a) Ptychography set-up (b) raster scan pattern

FIG. 1. *Simplified ptychographic set-up showing a Cartesian grid used for the overlapping raster scan positions* [24].

In particular, empirical evidence repeatedly points to the pitfalls of the raster scan, which is experimentally the easiest to implement [14] (Figure 1(b)). Raster scanning refers to the positions of the window function. The raster scan scheme is susceptible to periodic artifacts, known as *raster grid pathology*, attributed to the regularity and symmetry of the scan positions [35].

On the other hand, to the best of our knowledge, raster grid pathology has not been precisely formulated and analyzed. The purpose of the present work is a complete analysis of raster grid pathology from the perspective of uniqueness of the inverse problem. Uniqueness of solution is fundamental to any inverse problem. The exceptions to uniqueness are the ambiguities of the inverse problem. We identify the raster grid pathology reported in the optics literature as *periodic* ambiguities of period equal to the step size of the raster scan. Moreover, we will characterize all the other ambiguities inherent to the raster scan ptychography and consider a simple modification that can eliminate all the ambiguities except for those inherent to *any* blind ptychography.

Note that raster grid pathology only appears in blind ptychography but not in ptychography with a known probe. If the known probe is randomly phased and the adjacent probes overlap sufficiently, then the only ambiguity is a negligible constant phase factor [3].

Also there are two ambiguities inherent to any blind ptychography: a scaling factor and an affine phase factor. To give a precise description, we introduce some notation as follows.

Let $\mathbb{Z}_n^2 = [\![0, n-1]\!]^2$ be the object domain containing the support of the discrete object f, where $[\![k, l]\!]$ denotes the integers between, and including, $k \le l \in \mathbb{Z}$. Let $\mathcal{M}^{00} := \mathbb{Z}_m^2, m < n$, be the initial probe area, i.e., the support of the probe μ^{00} describing the illumination field. Here n is the global scale and m the intermediate scale of the set-up.

Let $\mathcal{T}$ be the set of all shifts, including $(0,0)$, involved in the ptychographic measurement. Denote by $\mu^{\mathbf{t}}$ the $\mathbf{t}$-shifted probe for all $\mathbf{t} \in \mathcal{T}$ and $\mathcal{M}^{\mathbf{t}}$ the domain of $\mu^{\mathbf{t}}$. Let $f^{\mathbf{t}}$ the object restricted to $\mathcal{M}^{\mathbf{t}}$. We refer to each $f^{\mathbf{t}}$ as a part of f and write $f = \vee_{\mathbf{t}} f^{\mathbf{t}}$, where $\vee$ is the "union" of functions consistent over their common support set. In ptychography, the original object is broken up into a set of overlapping object parts, each of which produces a $\mu^{\mathbf{t}}$-coded diffraction pattern. The totality of the coded diffraction patterns is called the ptychographic measurement data. Let ν^{00} (with $\mathbf{t} = (0,0)$) and $g = \vee_{\mathbf{t}} g^{\mathbf{t}}$ be any pair of the probe and the object estimates

producing the same ptychography data as μ^{00} and f, i.e., the diffraction pattern of $\nu^{\mathbf{t}} \odot g^{\mathbf{t}}$ is identical to that of $\mu^{\mathbf{t}} \odot f^{\mathbf{t}}$, where $\nu^{\mathbf{t}}$ is the $\mathbf{t}$-shift of ν^{00} and $g^{\mathbf{t}}$ is the restriction of g to $\mathcal{M}^{\mathbf{t}}$. For convenience, we assume the value zero for $\mu^{\mathbf{t}}, f^{\mathbf{t}}, \nu^{\mathbf{t}}, g^{\mathbf{t}}$ outside of $\mathcal{M}^{\mathbf{t}}$ and the periodic boundary condition on $\mathbb{Z}_n^2$ when $\mu^{\mathbf{t}}$ crosses over the boundary of $\mathbb{Z}_n^2$.

Consider the probe and object estimates

$$\nu^{00}(\mathbf{n}) = \mu^{00}(\mathbf{n}) \exp(-\mathrm{i}a - \mathrm{i}\mathbf{w} \cdot \mathbf{n}), \quad \mathbf{n} \in \mathcal{M}^{00}, \tag{1}$$

$$g(\mathbf{n}) = f(\mathbf{n}) \exp(\mathrm{i}b + \mathrm{i}\mathbf{w} \cdot \mathbf{n}), \quad \mathbf{n} \in \mathbb{Z}_n^2, \tag{2}$$

for any $a, b \in \mathbb{R}$ and $\mathbf{w} \in \mathbb{R}^2$. For any $\mathbf{t}$, we have the calculation

$$\begin{aligned} \nu^{\mathbf{t}}(\mathbf{n}) &= \nu^{00}(\mathbf{n} - \mathbf{t}) \\ &= \mu^{00}(\mathbf{n} - \mathbf{t}) \exp(-\mathrm{i}\mathbf{w} \cdot (\mathbf{n} - \mathbf{t})) \exp(-\mathrm{i}a) \\ &= \mu^{\mathbf{t}}(\mathbf{n}) \exp(-\mathrm{i}\mathbf{w} \cdot (\mathbf{n} - \mathbf{t})) \exp(-\mathrm{i}a) \end{aligned}$$

and hence for all $\mathbf{n} \in \mathcal{M}^{\mathbf{t}}, \mathbf{t} \in \mathcal{T}$,

$$\nu^{\mathbf{t}}(\mathbf{n}) g^{\mathbf{t}}(\mathbf{n}) = \mu^{\mathbf{t}}(\mathbf{n}) f^{\mathbf{t}}(\mathbf{n}) \exp(\mathrm{i}(b - a)) \exp(\mathrm{i}\mathbf{w} \cdot \mathbf{t}). \tag{3}$$

Clearly, (3) implies that g and ν^{00} produce the same ptychographic data as f and μ^{00} since for each $\mathbf{t}$, $\nu^{\mathbf{t}} \odot g^{\mathbf{t}}$ is a constant phase factor times $\mu^{\mathbf{t}} \odot f^{\mathbf{t}}$, where $\odot$ is the entrywise (Hadamard) product.

In addition to the affine phase ambiguity (1)–(2), another ambiguity, a scaling factor ($g = cf, \nu^{00} = c^{-1}\mu^{00}, c > 0$), is also inherent to any blind ptychography as can easily be checked. We refer to the scaling factor and the affine phase ambiguity as the inherent ambiguities of blind ptychography. Note that when the probe is exactly known $\nu^{00} = \mu^{00}$, neither ambiguity can occur.

A recent theory of uniqueness for blind ptychography with random probes [9] establishes that for general sampling schemes and with high probability (in the selection of the random probe), we have the relation

$$\nu^{\mathbf{t}} \odot g^{\mathbf{t}} = e^{\mathrm{i}\theta_{\mathbf{t}}} \mu^{\mathbf{t}} \odot f^{\mathbf{t}}, \quad \mathbf{t} \in \mathcal{T}, \tag{4}$$

for some constants $\theta_{\mathbf{t}} \in \mathbb{R}$ (called block phases here) if g and $\nu^{\mathbf{t}}$ produce the same diffraction pattern as f and $\mu^{\mathbf{t}}$ for all $\mathbf{t} \in \mathcal{T}$. The masked object parts $w^{\mathbf{t}} := \mu^{\mathbf{t}} \odot f^{\mathbf{t}}$ are also known as the *exit waves* in the scanning transmission electron microscopy literature.

We refer to (4) as the *local uniqueness* of the exit waves which means unique determination of the exit waves up to the block phases but not globally since $\theta_{\mathbf{t}}$ can depend on $\mathbf{t}$ and vary from block to block. However, the block phase profile is not arbitrary. For example, block phases for the raster scan always form an arithmetic progression (Theorem 3.1), possessing two degrees of freedom.

Once the exit waves $\psi^{\mathbf{t}}$ are determined up to block phases, relation (4) with $\theta_{\mathbf{t}}$ treated as parameters represents a bilinear system (in ν^{00} and g) of $m^2 \times |\mathcal{T}|$ equations coupled through the overlap between adjacent blocks. The total number of complex variables is $n^2 + m^2$. In the case of raster scan with step size τ, $|\mathcal{T}| \approx n^2/\tau^2$ and $m^2|\mathcal{T}| \approx n^2(\tau/m)^{-2}$, where the shift ratio τ/m is 1 minus the overlap ratio $(m-\tau)/m$. For 50% overlap ratio and $m < n$, $m^2|\mathcal{T}| \approx 4n^2$, a couple times larger than $(n^2 + m^2)$. This speaks of the potential redundancy of information in (4) on dimension count. Yet this simplistic analysis is deceptive as we will see that due to degenerate coupling

the raster scan has ambiguities of exactly τ^2+2 degrees of freedom in addition to the three degrees of freedom of the inherent ambiguities discussed above.

We will take (4) as the starting point of our analysis of raster scan ambiguities. We refer to any pair (ν^{00}, g) that satisfy (4) as a *ptychographic solution* and (μ^{00}, f) the *true solution*. Any ptychographic solution other than the true one is an ambiguity of blind ptychography. As noted above, the ambiguities of a constant scaling factor and affine phase factor are inherent to any blind ptychographic scheme. In this paper we aim first to characterize all the other ambiguities in the raster scan and, second, to show how to harness the nonlinear intermediate-scale coupling in (4) by more nuanced schemes with pixel-scale changes to totally eradicate ambiguities other than the inherent ones.

Throughout the paper, we make the convenient assumption of a nonvanishing probe (i.e., $\mu^{00}(\mathbf{n}) \neq 0$ for all $\mathbf{n} \in \mathcal{M}^{00}$) which is not strictly necessary. Physically speaking, a nonvanishing probe is transparent and casts no shadow on the object. On the other hand, as vanishing probe pixels would destroy the information of the corresponding object pixels (by multiplication) certain restriction on the pattern of vanishing probe pixels is inevitable, the stronger the restriction the smaller the overlapping ratio.

1.1. Our contribution. We first prove that the block phases of the raster scan of any step size $\tau < m$ always have an affine profile (section 3, Theorem 3.1). We then give a complete characterization of the raster scan ambiguities (Theorem 4.3).

Roughly speaking, there are two types of ambiguities besides the inherent ambiguities. First, there is the nonperiodic, arithmetically progressing ambiguity, inherited from the aforementioned affine block phase profile, which varies on the block scale, while the affine phase ambiguity varies on the pixel scale.

Second, there are τ-periodic ambiguities of τ^2 degrees of freedom, which we identify as a mathematical description of the raster grid pathology reported in the optics literature, i.e., the larger the step size the (much) more severe the raster scan pathology which cannot be removed without extra prior information.

Finally we demonstrate a simple mechanism for eliminating all the other ambiguities except the scaling factor and the affine phase ambiguity by slightly perturbing the raster scan with the minimum overlap ratio roughly 50%, consistent with experimental findings in the optics literature (section 5, Theorem 5.5). The optimal trade-off between the speed of data acquisition and the convergence rate of reconstruction lies in the balance between the average step size and the overlap size.

The rest of the paper is organized as follows. In section 2, we give a detailed presentation of the raster scan. In section 3, we prove that the block phases have an affine profile. In section 4, we give a complete characterization of the raster scan ambiguities. In section 5 we show that slightly perturbed raster scan has no other ambiguities than the scaling factor and the affine phase ambiguity. In section 6, we give a numerical demonstration of the perturbed raster scan. We conclude with a few remarks in section 7.

2. Raster scan. In this section, we give a precise formulation of the standard raster scans with various step sizes. In particular, we distinguish two cases: the undershifting schemes with an overlap ratio greater than 50% and the overshifting schemes with an overlap ratio less than 50%.

The raster scan can be formulated as the two-dimensional (2D) lattice with the basis $\{\mathbf{v}_1, \mathbf{v}_2\}$,

$$\mathcal{T} = \{\mathbf{t}_{kl} \equiv k\mathbf{v}_1 + l\mathbf{v}_2 : k, l \in \mathbb{Z}\}, \quad \mathbf{v}_1, \mathbf{v}_2 \in \mathbb{Z}^2, \tag{5}$$

acting on the object domain $\mathbb{Z}_n^2$. Instead of $\mathbf{v}_1$ and $\mathbf{v}_2$ we can also take $\mathbf{u}_1 = \ell_{11}\mathbf{v}_1 + \ell_{12}\mathbf{v}_2$ and $\mathbf{u}_2 = \ell_{21}\mathbf{v}_1 + \ell_{22}\mathbf{v}_2$ for integers ℓ_{ij} with $\ell_{11}\ell_{22} - \ell_{12}\ell_{21} = \pm 1$. This ensures that $\mathbf{v}_1$ and $\mathbf{v}_2$ themselves are integer linear combinations of $\mathbf{u}_1, \mathbf{u}_2$. Every lattice basis defines a fundamental parallelogram, which determines the lattice. There are five 2D lattice types, called period lattices, as given by the crystallographic restriction theorem. In contrast, there are 14 lattice types in three dimensions, called Bravais lattices [4].

We will focus on the simplest raster scan corresponding to the *square lattice* with $\mathbf{v}_1 = (\tau, 0), \mathbf{v}_2 = (0, \tau)$ of step size $\tau \in \mathbb{N}$. Our results can easily be extended to other lattice schemes.

Under the periodic boundary condition the raster scan with the step size $\tau = n/q, q \in \mathbb{N}$, $\mathcal{T}$ consists of $\mathbf{t}_{kl} = \tau(k, l)$, with $k, l \in \{0, 1, \dots, q-1\}$. The periodic boundary condition means that for $k = q-1$ or $l = q-1$ the shifted probe is wrapped around into the other end of the object domain. Denote the $\mathbf{t}_{kl}$-shifted probes and blocks by μ^{kl} and $\mathcal{M}^{kl}$, respectively. Likewise, denote by f^{kl} the object restricted to the shifted domain $\mathcal{M}^{kl}$.

Depending on whether $\tau \le m/2$ (the undershifting case) or $\tau > m/2$ (the overshifting case), we have two types of schemes. For the former case, all pixels of the object participate in an equal number of diffraction patterns. For the latter case, however, $4(m-\tau)^2$ pixels participate in four, $4(2\tau - m)(m-\tau)$ pixels participate in two, and $(2\tau - m)^2$ pixels participate in only one diffraction pattern, resulting in uneven coverage of the object.

2.1. The undershifting scheme $\tau \le m/2$. For simplicity of presentation we consider the case of $\tau = m/p$ for some integer $p \ge 2$ (i.e., $pn = qm$). As noted above, all pixels of the object participate in the same number (i.e., $2p$) of diffraction patterns. The borderline case $\tau = m/2$ (dubbed the minimalist scheme in [3]) corresponds to $p = 2$.

We partition the cyclical $\mathbf{t}^{kl}$-shifted probe μ^{kl} and the corresponding domain into equal-sized square blocks as

$$\mu^{kl} = \begin{bmatrix} \mu_{00}^{kl} & \mu_{10}^{kl} & \cdots & \mu_{p-1,0}^{kl} \\ \mu_{01}^{kl} & \mu_{11}^{kl} & \cdots & \mu_{p-1,1}^{kl} \\ \vdots & \vdots & \vdots & \vdots \\ \mu_{0,p-1}^{kl} & \mu_{1,p-1}^{kl} & \cdots & \mu_{p-1,p-1}^{kl} \end{bmatrix}, \quad \mu_{ij}^{kl} \in \mathbb{C}^{m/p \times m/p}, \tag{6}$$

$$\mathcal{M}^{kl} = \begin{bmatrix} \mathcal{M}_{00}^{kl} & \mathcal{M}_{10}^{kl} & \cdots & \mathcal{M}_{p-1,0}^{kl} \\ \mathcal{M}_{01}^{kl} & \mathcal{M}_{11}^{kl} & \cdots & \mathcal{M}_{p-1,1}^{kl} \\ \vdots & \vdots & \vdots & \vdots \\ \mathcal{M}_{0,p-1}^{kl} & \mathcal{M}_{1,p-1}^{kl} & \cdots & \mathcal{M}_{p-1,p-1}^{kl} \end{bmatrix}, \quad \mathcal{M}_{ij}^{kl} \in \mathbb{Z}^{m/p \times m/p}, \tag{7}$$

under the periodic boundary condition

$$\mu_{j,l}^{q-1-i,k} = \mu_{j-i-1,l}^{0k}, \quad \mu_{l,j}^{k,q-1-i} = \mu_{l,j-i-1}^{k0}, \tag{8}$$

$$\mathcal{M}_{j,l}^{q-1-i,k} = \mathcal{M}_{j-i-1,l}^{0k}, \quad \mathcal{M}_{l,j}^{k,q-1-i} = \mathcal{M}_{l,j-i-1}^{k0} \tag{9}$$

for all $0 \le i \le j-1 \le p-2, k = 1, \dots, q-1, l = 1, \dots, p-1$.

Accordingly, we divide the object f into q^2 nonoverlapping square blocks

$$f = \begin{bmatrix} f_{00} & \cdots & f_{q-1,0} \\ \vdots & \vdots & \vdots \\ f_{0,q-1} & \cdots & f_{q-1,q-1} \end{bmatrix}, \quad f_{ij} \in \mathbb{C}^{m/p \times m/p}. \tag{10}$$

2.2. The overshifting scheme $\tau > m/2$. Because of uneven coverage of the object domain, the over-shifting case is more complicated.

We divide the shifted probe μ^{kl} and its domain as

$$\mu^{kl} = \begin{bmatrix} \mu^{kl}_{00} & \mu^{kl}_{10} & \mu^{kl}_{20} \\ \mu^{kl}_{01} & \mu^{kl}_{11} & \mu^{kl}_{21} \\ \mu^{kl}_{02} & \mu^{kl}_{12} & \mu^{kl}_{22} \end{bmatrix} \in \mathbb{C}^{m\times m}, \tag{11}$$

$$\mathcal{M}^{kl} = \begin{bmatrix} \mathcal{M}^{kl}_{00} & \mathcal{M}^{kl}_{10} & \mathcal{M}^{kl}_{20} \\ \mathcal{M}^{kl}_{01} & \mathcal{M}^{kl}_{11} & \mathcal{M}^{kl}_{21} \\ \mathcal{M}^{kl}_{02} & \mathcal{M}^{kl}_{12} & \mathcal{M}^{kl}_{22} \end{bmatrix} \in \mathbb{Z}^{m\times m} \tag{12}$$

under the periodic boundary condition

$$\mathcal{M}^{q-1,k}_{2j} = \mathcal{M}^{0k}_{0j} \quad \mathcal{M}^{k,q-1}_{i2} = \mathcal{M}^{k0}_{i0}, \tag{13}$$

$$\mu^{q-1,k}_{2j} = \mu^{0k}_{0j}, \quad \mu^{k,q-1}_{i2} = \mu^{k0}_{i0}, \tag{14}$$

for all $k = 1, \dots, q-1$ and $i, j = 0, 1, 2$, where q is the number of shifts in each direction.

Note that the sizes of these blocks are not equal: the four corner blocks are $(m-\tau)\times(m-\tau)$, the center block is $(2\tau - m)\times(2\tau - m)$, and the rest are either $(2\tau - m)\times(m-\tau)$ or $(m-\tau)\times(2\tau - m)$. As a result, the corresponding partition of f also has unequally sized blocks.

We write

$$f = \bigvee_{k,l=0}^{q-1} f^{kl}, \quad f^{kl} = \begin{bmatrix} f^{kl}_{00} & f^{kl}_{10} & f^{kl}_{20} \\ f^{kl}_{01} & f^{kl}_{11} & f^{kl}_{21} \\ f^{kl}_{02} & f^{kl}_{12} & f^{kl}_{22} \end{bmatrix} \in \mathbb{C}^{m\times m}, \tag{15}$$

where, for $i, j = 0, 1, 2,\ k, l = 0, \dots, q-1$,

$$f^{kl}_{2j} = f^{k+1,l}_{0j}, \quad f^{k,l}_{i2} = f^{k,l+1}_{i0}.$$

3. Affine block phases. Let S be any cyclic subgroup of $\mathcal{T}$ generated by $\mathbf{v}$, i.e., $S := \{\mathbf{t}_j = j\mathbf{v} : j = 0, \dots, s-1\}$, of order s, i.e., $s\mathbf{v} = 0 \mod n$. For ease of notation, denote by μ^k, f^k, ν^k, g^k, and M^k for the respective $\mathbf{t}_k$-shifted quantities.

THEOREM 3.1. *As in* (4)*, suppose that*

$$\nu^k \odot g^k = e^{\mathrm{i}\theta_k} \mu^k \odot f^k, \quad k = 0, \dots, s-1, \tag{16}$$

where μ^k and ν^k vanish nowhere in $\mathcal{M}^k$. If, for all $k = 0, \dots, s-1$,

$$\mathcal{M}^k \cap \mathcal{M}^{k+1} \cap \mathrm{supp}(f) \cap (\mathrm{supp}(f) + \mathbf{v}) \neq \emptyset, \tag{17}$$

then the sequence $\{\theta_0, \theta_1, \dots, \theta_{s-1}\}$ is an arithmetic progression where $\Delta\theta = \theta_k - \theta_{k-1}$ is an integer multiple of $2\pi/s$.

Remark 3.2. If f has a full support, i.e., $\mathrm{supp}(f) = \mathbb{Z}_n^2$, then (17) holds for any step size $\tau < m$ (i.e., positive overlap).

Proof. Rewriting (16) in the form

$$\nu^{k+1}(\mathbf{n})g^{k+1}(\mathbf{n}) = e^{\mathrm{i}\theta_{k+1}}\mu^{k+1}(\mathbf{n})f^{k+1}(\mathbf{n}) \tag{18}$$

and substituting (16) into (18) for $\mathbf{n} \in \mathcal{M}^k \cap \mathcal{M}^{k+1}$, we have

$$e^{\mathrm{i}\theta_k} f^k(\mathbf{n})\mu^k(\mathbf{n})/\nu^k(\mathbf{n}) = e^{\mathrm{i}\theta_{k+1}} f^{k+1}(\mathbf{n})\mu^{k+1}(\mathbf{n})/\nu^{k+1}(\mathbf{n})$$

and hence for all $\mathbf{n} \in \mathcal{M}^k \cap \mathcal{M}^{k+1} \cap \operatorname{supp}(f)$,

$$e^{\mathrm{i}\theta_k}\mu^k(\mathbf{n})/\nu^k(\mathbf{n}) = e^{\mathrm{i}\theta_{k+1}}\mu^{k+1}(\mathbf{n})/\nu^{k+1}(\mathbf{n}). \tag{19}$$

For all $j = 0, \dots, s-1$, substituting

$$\nu^j(\mathbf{n}) = \nu^{j+1}(\mathbf{n}+\mathbf{v}), \quad \mu^j(\mathbf{n}) = \mu^{j+1}(\mathbf{n}+\mathbf{v}), \tag{20}$$

into (19), we have that for $\mathbf{n} \in \mathcal{M}^k \cap \mathcal{M}^{k+1} \cap \operatorname{supp}(f)$

$$\begin{aligned} &e^{\mathrm{i}\theta_k}\mu^{k+1}(\mathbf{n}+\mathbf{v})/\nu^{k+1}(\mathbf{n}+\mathbf{v}) \\ &= e^{\mathrm{i}\theta_{k+1}}\mu^{k+2}(\mathbf{n}+\mathbf{v})/\nu^{k+2}(\mathbf{n}+\mathbf{v}), \end{aligned}$$

or equivalently

$$\begin{aligned} e^{\mathrm{i}\theta_k}\mu^{k+1}(\mathbf{n})/\nu^{k+1}(\mathbf{n}) &= e^{\mathrm{i}\theta_{k+1}}\mu^{k+2}(\mathbf{n})/\nu^{k+2}(\mathbf{n}), \\ &\forall \mathbf{n} \in \mathcal{M}^{k+1} \cap \mathcal{M}^{k+2} \cap (\operatorname{supp}(f) + \mathbf{v}) \end{aligned} \tag{21}$$

On the other hand, (19) also implies

$$\begin{aligned} e^{\mathrm{i}\theta_{k+1}}\mu^{k+1}(\mathbf{n})/\nu^{k+1}(\mathbf{n}) &= e^{\mathrm{i}\theta_{k+2}}\mu^{k+2}(\mathbf{n})/\nu^{k+2}(\mathbf{n}), \\ &\forall \mathbf{n} \in \mathcal{M}^{k+1} \cap \mathcal{M}^{k+2} \cap \operatorname{supp}(f). \end{aligned} \tag{22}$$

Hence, if

$$\mathcal{M}^k \cap \mathcal{M}^{k+1} \cap \operatorname{supp}(f) \cap (\operatorname{supp}(f) + \mathbf{v}) \neq \emptyset,$$

then (22) and (21) imply that

$$e^{\mathrm{i}\theta_{k+1}} e^{-\mathrm{i}\theta_k} = e^{\mathrm{i}\theta_k} e^{-\mathrm{i}\theta_{k-1}} \quad \forall k = 0, \dots, s-1 \tag{23}$$

and hence $\Delta\theta = \theta_k - \theta_{k-1}$ is independent of k. In other words, $\{\theta_0, \theta_1, \theta_2 \dots\}$ is an arithmetic progression.

Moreover, the periodic boundary condition and the fact that $s\mathbf{v} = 0 \mod 2\pi$ imply that $s\Delta\theta$ is an integer multiple of 2π. ∎

Applying Theorem 3.1 to the two-generator square lattice group $\mathcal{T}$ we have the following result.

COROLLARY 3.3. *For the full raster scan $\mathcal{T}$, the block phases have the profile*

$$\theta_{kl} = \theta_{00} + \mathbf{r} \cdot (k, l), \quad k, l = 0, \dots, q-1, \tag{24}$$

for some $\theta_{00} \in \mathbb{R}$ and $\mathbf{r} = (r_1, r_2)$, where r_1 and r_2 are integer multiples of $2\pi/q$.

4. Raster scan ambiguities. In this section we give a complete characterization of the raster scan ambiguities other than the scaling factor and the affine phase ambiguity (1)–(2), including the arithmetically progressing phase factor inherited from the block phases and the raster grid pathology which has a τ-periodic structure of $\tau \times \tau$ degrees of freedom. We will resume the set-up of section 2.

Before we state the general result. Let us consider two examples of the undershifting schemes to illustrate each type of ambiguity separately.

The first example shows an ambiguity resulting from the arithmetically progressing block phases which make positive and negative imprints on the object and phase estimates, respectively.

Example 4.1. For $q = 3, \tau = m/2$, let

$$f = \begin{bmatrix} f_{00} & f_{10} & f_{20} \\ f_{01} & f_{11} & f_{21} \\ f_{02} & f_{12} & f_{22} \end{bmatrix},$$
$$g = \begin{bmatrix} f_{00} & e^{\mathrm{i}2\pi/3} f_{10} & e^{\mathrm{i}4\pi/3} f_{20} \\ e^{\mathrm{i}2\pi/3} f_{01} & e^{\mathrm{i}4\pi/3} f_{11} & f_{21} \\ e^{\mathrm{i}4\pi/3} f_{02} & f_{12} & e^{\mathrm{i}2\pi/3} f_{22} \end{bmatrix}$$

be the object and its reconstruction, respectively, where $f_{ij} \in \mathbb{C}^{n/3 \times n/3}$. Let

$$\mu^{kl} = \begin{bmatrix} \mu_{00}^{kl} & \mu_{10}^{kl} \\ \mu_{01}^{kl} & \mu_{11}^{kl} \end{bmatrix}, \quad \nu^{kl} = \begin{bmatrix} \mu_{00}^{kl} & e^{-\mathrm{i}2\pi/3} \mu_{10}^{kl} \\ e^{-\mathrm{i}2\pi/3} \mu_{01}^{kl} & e^{-\mathrm{i}4\pi/3} \mu_{11}^{kl} \end{bmatrix},$$

$k, l = 0, 1, 2$, be the (k, l)th shift of the probe and estimate, respectively, where $\mu_{ij}^{kl} \in \mathbb{C}^{n/3 \times n/3}$.

Let f^{ij} and g^{ij} be the part of the object and estimate illuminated by μ^{ij} and ν^{ij}, respectively. For example, we have

$$f^{00} = \begin{bmatrix} f_{00} & f_{10} \\ f_{01} & f_{11} \end{bmatrix}, \quad f^{10} = \begin{bmatrix} f_{10} & f_{20} \\ f_{11} & f_{21} \end{bmatrix}, \quad f^{20} = \begin{bmatrix} f_{20} & f_{00} \\ f_{21} & f_{01} \end{bmatrix}$$

and likewise for other f^{ij} and g^{ij}. It is easily seen that $\nu^{ij} \odot g^{ij} = e^{\mathrm{i}(i+j)2\pi/3} \mu^{ij} \odot f^{ij}$.

The next example illustrates the periodic artifact called raster grid pathology.

Example 4.2. For $q = 3, \tau = m/2$, and any $\psi \in \mathbb{C}^{\frac{n}{3} \times \frac{n}{3}}$, let

$$f = \begin{bmatrix} f_{00} & f_{10} & f_{20} \\ f_{01} & f_{11} & f_{21} \\ f_{02} & f_{12} & f_{22} \end{bmatrix},$$
$$g = \begin{bmatrix} e^{-\mathrm{i}\psi} \odot f_{00} & e^{-\mathrm{i}\psi} \odot f_{10} & e^{-\mathrm{i}\psi} \odot f_{20} \\ e^{-\mathrm{i}\psi} \odot f_{01} & e^{-\mathrm{i}\psi} \odot f_{11} & e^{-\mathrm{i}\psi} \odot f_{21} \\ e^{-\mathrm{i}\psi} \odot f_{02} & e^{-\mathrm{i}\psi} \odot f_{12} & e^{-\mathrm{i}\psi} \odot f_{22} \end{bmatrix}$$

be the object and its reconstruction, respectively, where $f_{ij} \in \mathbb{C}^{n/3 \times n/3}$. Let

$$\mu^{kl} = \begin{bmatrix} \mu_{00}^{kl} & \mu_{10}^{kl} \\ \mu_{01}^{kl} & \mu_{11}^{kl} \end{bmatrix}, \quad \nu^{kl} = \begin{bmatrix} e^{\mathrm{i}\psi} \odot \mu_{00}^{kl} & e^{\mathrm{i}\psi} \odot \mu_{10}^{kl} \\ e^{\mathrm{i}\psi} \odot \mu_{01}^{kl} & e^{\mathrm{i}\psi} \odot \mu_{11}^{kl} \end{bmatrix},$$

$k, l = 0, 1, 2$, be the (k, l)th shift of the probe and estimate, respectively, where $\mu_{ij}^{kl} \in \mathbb{C}^{n/3 \times n/3}$.

Let f^{ij} and g^{ij} be the part of the object and estimate illuminated by μ^{ij} and ν^{ij}, respectively (as in Example 4.1). It is verified easily that $\nu^{ij} \odot g^{ij} = \mu^{ij} \odot f^{ij}$.

The combination of the above two types of ambiguity gives rise to the general ambiguities for blind ptychography with the raster scan as stated next.

THEOREM 4.3. *Let* $\operatorname{supp}(f) = \mathbb{Z}_n^2$. *Consider the raster scan* $\mathcal{T}$ *and suppose that an object estimate* g *and a probe estimate* ν^{00} *satisfy the relation*

$$\nu^{kl} \odot g^{kl} = e^{\mathrm{i}\theta_{kl}} \mu^{kl} \odot f^{kl}, \quad \theta_{kl} = \theta_{00} + \mathbf{r} \cdot (k, l) \tag{25}$$

as given by Theorem 3.1 *where* μ^{kl} *and* ν^{kl} *vanish nowhere for all* k, l.

The following statements hold.

(I) *For* $\tau \le m/2$, *if, for any* $\psi \in \mathbb{C}^{\tau \times \tau}$,

$$\nu_{00}^{00} = e^{\mathrm{i}\psi} \odot \mu_{00}^{00}, \tag{26}$$

then

$$\nu_{kl}^{00} = e^{-\mathrm{i}\mathbf{r}\cdot(k,l)} e^{\mathrm{i}\psi} \odot \mu_{kl}^{00}, \quad k, l = 0, \dots, p-1, \tag{27}$$

$$g_{kl} = e^{\mathrm{i}\theta_{00}} e^{\mathrm{i}\mathbf{r}\cdot(k,l)} e^{-\mathrm{i}\psi} \odot f_{kl}, \quad k, l = 0, \dots, q-1. \tag{28}$$

(II) *For* $\tau > m/2$, *if*

$$\begin{bmatrix} \nu_{00}^{00} & \nu_{10}^{00} \\ \nu_{01}^{00} & \nu_{11}^{00} \end{bmatrix} = e^{\mathrm{i}\psi} \odot \begin{bmatrix} \mu_{00}^{00} & \mu_{10}^{00} \\ \mu_{01}^{00} & \mu_{11}^{00} \end{bmatrix} \tag{29}$$

for any

$$\psi = \begin{bmatrix} \psi_{00} & \psi_{10} \\ \psi_{01} & \psi_{11} \end{bmatrix} \in \mathbb{C}^{\tau \times \tau},$$

then

$$\begin{bmatrix} g_{00}^{kl} & g_{10}^{kl} \\ g_{01}^{kl} & g_{11}^{kl} \end{bmatrix} = e^{\mathrm{i}\theta_{00}} e^{\mathrm{i}\mathbf{r}\cdot(k,l)} e^{-\mathrm{i}\psi} \odot \begin{bmatrix} f_{00}^{kl} & f_{10}^{kl} \\ f_{01}^{kl} & f_{11}^{kl} \end{bmatrix} \tag{30}$$

for all $k, l = 0, \dots, q-1$. *Moreover,*

$$\nu_{2j}^{00} = e^{-\mathrm{i}r_1} e^{\mathrm{i}\psi_{0j}} \odot \mu_{2j}^{00}, \quad j = 0, 1, \tag{31}$$

$$\nu_{j2}^{00} = e^{-\mathrm{i}r_2} e^{\mathrm{i}\psi_{j0}} \odot \mu_{j2}^{00}, \quad j = 0, 1, \tag{32}$$

$$\nu_{22}^{00} = e^{-\mathrm{i}(r_1+r_2)} e^{\mathrm{i}\psi_{00}} \odot \mu_{22}^{00} \tag{33}$$

and hence

$$g_{2j}^{kl} = e^{\mathrm{i}\theta_{00}} e^{\mathrm{i}\mathbf{r}\cdot(k+1,l)} e^{-\mathrm{i}\psi_{0j}} \odot f_{2j}^{kl}, \quad j = 0, 1, \tag{34}$$

$$g_{j2}^{kl} = e^{\mathrm{i}\theta_{00}} e^{\mathrm{i}\mathbf{r}\cdot(k,l+1)} e^{-\mathrm{i}\psi_{j0}} \odot f_{j2}^{kl}, \quad j = 0, 1, \tag{35}$$

$$g_{22}^{kl} = e^{\mathrm{i}\theta_{00}} e^{\mathrm{i}\mathbf{r}\cdot(k+1,l+1)} e^{-\mathrm{i}\psi_{00}} \odot f_{22}^{kl}. \tag{36}$$

Remark 4.4. Since ψ is any complex $\tau \times \tau$ matrix, (26) and (29) represent the maximum degrees of ambiguity over the respective initial subblocks. This ambiguity is transmitted to other subblocks, forming periodic artifacts called the raster grid pathology.

On top of the periodic artifacts, there is the nonperiodic ambiguity inherited from the affine block phase profile. The nonperiodic arithmetically progressing ambiguity is different from the affine phase ambiguity (1)–(2) as they manifest on different scales: the former is constant in each $\tau \times \tau$ block (indexed by k, l), while the latter varies from pixel to pixel.

Proof.

(I) For $\tau \le m/2$, recall the decomposition

$$\nu^{kl} = \begin{bmatrix} \nu^{kl}_{00} & \nu^{kl}_{10} & \cdots & \nu^{kl}_{p-1,0} \\ \nu^{kl}_{01} & \mu^{kl}_{11} & \cdots & \nu^{kl}_{p-1,1} \\ \vdots & \vdots & \vdots & \vdots \\ \nu^{kl}_{0,p-1} & \nu^{kl}_{1,p-1} & \cdots & \nu^{kl}_{p-1,p-1} \end{bmatrix}, \quad g = \begin{bmatrix} g_{00} & \cdots & g_{q-1,0} \\ \vdots & \vdots & \vdots \\ g_{0,q-1} & \cdots & g_{q-1,q-1} \end{bmatrix},$$

with $\nu^{kl}_{ij}, g_{ij} \in \mathbb{C}^{m/p \times m/p}$, in analogy to (6) and (10).

$$g_{00} = e^{\mathrm{i}\theta_{00}} e^{-\mathrm{i}\psi} \odot f_{00}$$

by restricting (25) to $\mathcal{M}^{00}_{00}$.
For $\mathbf{n} \in \mathcal{M}^{10}_{00}$, we have

$$\nu^{10}_{00} \odot g_{10} = e^{\mathrm{i}\theta_{10}} \mu^{10}_{00} \odot f_{10},$$

by (25), and

$$\nu^{10}_{00}(\mathbf{n}) = \nu^{00}_{00}(\mathbf{n} - (\tau, 0)) = \left(e^{\mathrm{i}\psi} \odot \mu^{00}_{00}\right)(\mathbf{n} - (\tau, 0)) = \left(e^{\mathrm{i}\psi} \odot \mu^{10}_{00}\right)(\mathbf{n})$$

by (26). Hence

$$g_{10} = e^{\mathrm{i}\theta_{10}} e^{-\mathrm{i}\psi} \odot f_{10}$$

implying

$$\nu^{00}_{10} \odot g_{10} = e^{\mathrm{i}\theta_{10}} e^{-\mathrm{i}\psi} \nu^{00}_{10} \odot f_{10} = e^{\mathrm{i}\theta_{00}} \mu^{00}_{10} \odot f_{10}$$

by (25) and consequently

$$\nu^{00}_{10} = e^{\mathrm{i}\theta_{00}} e^{-\mathrm{i}\theta_{10}} e^{\mathrm{i}\psi} \mu^{00}_{10}.$$

Repeating the same argument for the adjacent blocks in both directions, we obtain

$$\begin{aligned} \nu^{00}_{kl} &= e^{\mathrm{i}\theta_{00}} e^{-\mathrm{i}\theta_{kl}} e^{\mathrm{i}\psi} \odot \mu^{00}_{kl}, \\ g_{kl} &= e^{\mathrm{i}\theta_{kl}} e^{-\mathrm{i}\psi} \odot f_{kl}, \end{aligned}$$

which are equivalent to (27) and (28) in view of the block phase profile in (24).

(II) First recall

$$\mu^{kl} = \begin{bmatrix} \mu^{kl}_{00} & \mu^{kl}_{10} & \mu^{kl}_{20} \\ \mu^{kl}_{01} & \mu^{kl}_{11} & \mu^{kl}_{21} \\ \mu^{kl}_{02} & \mu^{kl}_{12} & \mu^{kl}_{22} \end{bmatrix}, \quad g = \bigvee_{k,l=0}^{q-1} g^{kl}, \quad g^{kl} = \begin{bmatrix} g^{kl}_{00} & g^{kl}_{10} & g^{kl}_{20} \\ g^{kl}_{01} & g^{kl}_{11} & g^{kl}_{21} \\ g^{kl}_{02} & g^{kl}_{12} & g^{kl}_{22} \end{bmatrix}$$

in analogy to (11) and (15).

Since

$$\nu^{kl}(\mathbf{n}) = \nu^{00}(\mathbf{n} - \tau(k,l))), \quad \mu^{kl}(\mathbf{n}) = \mu^{00}(\mathbf{n} - \tau(k,l)), \tag{37}$$

(30) follows from (29) and (25).

By (29) and restricting (25) to $\mathcal{M}^{10}_{0j}, j = 0, 1$, we obtain

$$g^{00}_{2j} = g^{10}_{0j} = e^{\mathrm{i}\theta_{10}} e^{-\mathrm{i}\psi_{0j}} \odot f^{10}_{0j} = e^{\mathrm{i}\theta_{10}} e^{-\mathrm{i}\psi_{0j}} \odot f^{00}_{2j}, \quad j = 0, 1,$$

which implies by (25)

$$\nu^{00}_{2j} = e^{\mathrm{i}\theta_{00}} e^{-\mathrm{i}\theta_{10}} e^{\mathrm{i}\psi_{0j}} \odot \mu^{00}_{2j}, \quad j = 0, 1,$$
$$\nu^{00}_{j2} = e^{\mathrm{i}\theta_{00}} e^{-\mathrm{i}\theta_{01}} e^{\mathrm{i}\psi_{j0}} \odot \mu^{00}_{j2}, \quad j = 0, 1,$$

and consequently (31) and (32).

By (37) and restricting (25) to $\mathcal{M}^{kl}_{2j}, \mathcal{M}^{kl}_{j2}, j = 0, 1$, we have (34) and (35).

For (36) with $(k,l) = (0,0)$, the block $\mathcal{M}^{10}_{02} = \mathcal{M}^{00}_{22}$ is masked by μ^{10}_{02}, a translate of μ^{00}_{02}. By restricting (25) to $\mathcal{M}^{10}_{02}$,

$$g^{00}_{22} = g^{10}_{02} = e^{\mathrm{i}(\theta_{10} + \theta_{01} - \theta_{00})} e^{-\mathrm{i}\psi_{00}} \odot f^{00}_{22}, \tag{38}$$

which is equivalent to (36) with $(k,l) = (0,0)$. Then (25) and (38) imply

$$\nu^{00}_{22} = e^{\mathrm{i}(\theta_{00} - \theta_{10})} e^{\mathrm{i}(\theta_{00} - \theta_{01})} e^{\mathrm{i}\psi_{00}} \odot \mu^{00}_{22}, \tag{39}$$

which is equivalent to (33).

For general k, l, (33) becomes

$$\nu^{kl}_{22} = e^{-\mathrm{i}(r_1 + r_2)} e^{\mathrm{i}\psi_{00}} \odot \mu^{kl}_{22}. \tag{40}$$

By (40) and restricting (25) to $\mathcal{M}^{kl}_{22}$ we have

$$g^{kl}_{22} = e^{\mathrm{i}\theta_{kl}} e^{\mathrm{i}(r_1 + r_2)} e^{-\mathrm{i}\psi_{00}} \odot f^{kl}_{22}$$

and hence (36). ∎

When $\tau = 1$, the nonperiodic, arithmetically progressing ambiguity and the affine phase ambiguity become the same. In addition, for $\tau = 1$ the raster grid pathology becomes a constant phase factor which can be ignored [17].

COROLLARY 4.5. *If $\tau = 1$ (i.e., $q = n, p = m$) and (25) holds, then the probe and the object can be uniquely and simultaneously determined.*

Proof. For $\tau = 1$, μ_{00} consists of just one pixel and ψ is a number. Hence $\mu^{00} = \nu^{00}$ up to a constant phase factor and (27)–(28) then imply that the affine phase ambiguity is the only ambiguity modulo the constant phase factor. ∎

5. Slightly perturbed raster scan. In this section, we demonstrate a simple way to remove all the raster scan ambiguities except for the scaling factor and the affine phase ambiguity.

For the rest of the paper, we assume that f does not vanish in $\mathbb{Z}^2_n$.

We consider the perturbed raster scan (Figure 2(a))

$$\mathbf{t}_{kl} = \tau(k,l) + (\delta^1_k, \delta^2_l), \quad k, l = 0, \ldots, q-1, \tag{41}$$

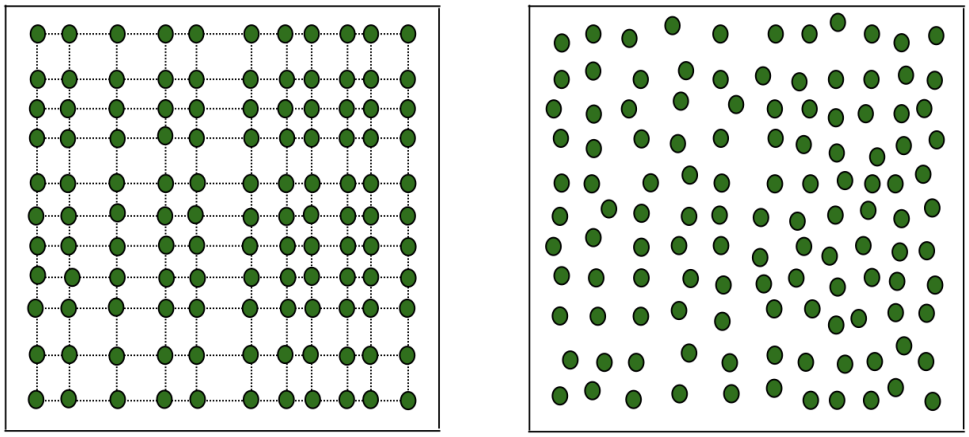

(a) Perturbed grid given by (41) (b) Perturbed grid given by (42)

FIG. 2. *Two perturbed raster scans.*

where δ_k^1, δ_l^2 are small integers relative to τ and $m-\tau$ (see Theorem 5.5 for details). More general than (41) is the perturbed grid pattern (Figure 2(b)),

$$\mathbf{t}_{kl} = \tau(k,l) + \left(\delta_{kl}^1, \delta_{kl}^2\right), \quad k,l = 0,\dots,q-1, \tag{42}$$

which is harder to analyze, and we will present numerical simulation to confirm its performance. Without loss of generality we set $\delta_0^1 = \delta_0^2 = 0$ and hence $\mathbf{t}_{00} = (0,0)$.

As before we assume that $\mathrm{supp}[\mu^{00}] = \mathrm{supp}[\nu^{00}] = \mathcal{M}^{00}$. Let us write the probe and object errors as

$$\nu^{00}(\mathbf{n})/\mu^{00}(\mathbf{n}) := \alpha(\mathbf{n})\exp\left(\mathrm{i}\phi(\mathbf{n})\right), \quad \mathbf{n} \in \mathcal{M}^{00}, \tag{43}$$

$$h(\mathbf{n}) := \ln g(\mathbf{n}) - \ln f(\mathbf{n}), \quad \mathbf{n} \in \mathbb{Z}_n^2, \tag{44}$$

where we assume $\alpha(\mathbf{n}) \neq 0$ for all $\mathbf{n} \in \mathcal{M}^{00}$, and rewrite (4) as

$$h(\mathbf{n}+\mathbf{t}) = \mathrm{i}\theta_{\mathbf{t}} - \ln\alpha(\mathbf{n}) - \mathrm{i}\phi(\mathbf{n}) \mod \mathrm{i}2\pi \tag{45}$$

for $\mathbf{n} \in \mathcal{M}^{00}$.

By (45) with $\mathbf{t} = (0,0)$,

$$h(\mathbf{n}) = \mathrm{i}\theta_{00} - \ln\alpha(\mathbf{n}) - \mathrm{i}\phi(\mathbf{n}) \quad \forall \mathbf{n} \in \mathcal{M}^{00} \tag{46}$$

and hence for all $\mathbf{t} \in \mathcal{T}$ and $\mathbf{n} \in \mathcal{M}^{00}$

$$h(\mathbf{n}+\mathbf{t}) - h(\mathbf{n}) = \mathrm{i}\theta_{\mathbf{t}} - \mathrm{i}\theta_{00} \mod \mathrm{i}2\pi. \tag{47}$$

We wish to generalize such a relationship to the case where $\mathbf{t}$ in (47) is replaced by $\mathbf{e}_1 = (1,0)$ and $\mathbf{e}_2 = (0,1)$.

5.1. A simple perturbation. Let us first study the simple example of the two-shift perturbation to the raster scan with $\delta_2^1 = \delta_2^2 = -1$ but all other $\delta_k^j = 0$, i.e., $\mathbf{t}_{kl} = \tau(k,l)$ for $(k,l) \neq (2,0),(0,2)$. Then

$$h(\mathbf{n} + 2\mathbf{t}_{10} - \mathbf{t}_{20}) = h(\mathbf{n}+(1,0)), \tag{48}$$

$$h(\mathbf{n} + 2\mathbf{t}_{01} - \mathbf{t}_{02}) = h(\mathbf{n}+(0,1)). \tag{49}$$

There are several routes of reduction from $(1,0)$ to $(0,0)$ via the shifts in $\mathcal{T}$. For example, we can proceed from $(1,0) = 2\mathbf{t}_{10} - \mathbf{t}_{20}$ to $(0,0)$ along the path

$$(2\mathbf{t}_{10} - \mathbf{t}_{20}) \longrightarrow (\mathbf{t}_{10} - \mathbf{t}_{20}) \longrightarrow \mathbf{t}_{10} \longrightarrow (0,0) \tag{50}$$

by repeatedly applying (47) where the direction of the second step is to be reversed since $-\mathbf{t}_{20} \notin \mathcal{T}$ ($\mathcal{T}$ is no longer a group even under the periodic boundary condition). The direction is important for keeping track of the domain of validity of (47) along the path. Hence for all

$$\mathbf{n} \in (\mathcal{M}^{00} + \mathbf{t}_{20} - \mathbf{t}_{10}) \cap \mathcal{M}^{00} \tag{51}$$

we have

$$\begin{aligned} h(\mathbf{n} + 2\mathbf{t}_{10} - \mathbf{t}_{20}) &= h(\mathbf{n} + \mathbf{t}_{10} - \mathbf{t}_{20}) + \mathrm{i}\theta_{10} - \mathrm{i}\theta_{00} \\ &= h(\mathbf{n} + \mathbf{t}_{10}) + \mathrm{i}\theta_{10} - \mathrm{i}\theta_{20} \\ &= h(\mathbf{n}) + 2\mathrm{i}\theta_{10} - \mathrm{i}\theta_{20} - \mathrm{i}\theta_{00} \end{aligned}$$

and hence

$$h(\mathbf{n} + (1,0)) = h(\mathbf{n}) + \mathrm{i}\Delta^1, \quad \Delta^1 := 2\theta_{10} - \theta_{20} - \theta_{00} \tag{52}$$

modulo $\mathrm{i}2\pi$.

Let us consider another alternative route for reduction:

$$(2\mathbf{t}_{10} - \mathbf{t}_{20}) \longrightarrow 2\mathbf{t}_{10} \longrightarrow \mathbf{t}_{10} \longrightarrow (0,0), \tag{53}$$

where the proper direction for the first step in applying (47) is reversed. Keeping track of the domain of validity along the path, we have

$$\begin{aligned} h(\mathbf{n} + 2\mathbf{t}_{10} - \mathbf{t}_{20}) &= h(\mathbf{n} + 2\mathbf{t}_{10}) - \mathrm{i}\theta_{20} + \mathrm{i}\theta_{00} \\ &= h(\mathbf{n} + \mathbf{t}_{10}) + \mathrm{i}\theta_{10} - \mathrm{i}\theta_{20} \\ &= h(\mathbf{n}) + \mathrm{i}\Delta^1 \end{aligned}$$

for all

$$\mathbf{n} \in (\mathcal{M}^{00} - 2\mathbf{t}_{10} + \mathbf{t}_{20}) \cap (\mathcal{M}^{00} - \mathbf{t}_{10}) \cap \mathcal{M}^{00}. \tag{54}$$

In summary, (52) holds for all $\mathbf{n}$ in the union of (51) and (54), i.e.,

$$D^1 = (\llbracket 0, m - \tau - 1 \rrbracket \cup \llbracket \tau - 1, m - 1 \rrbracket) \times \llbracket 0, m - 1 \rrbracket$$

provided that $\tau \geq 1$.

Including other routes for reducing $2\mathbf{t}_{10} - \mathbf{t}_{20}$ to $(1,0)$ in D^1 can enlarge the domain of validity for (52). For simplicity of argument, we omit them here.

By repeatedly applying (47) we have the following result.

PROPOSITION 5.1. *The relation* (52) *holds true in the set*

$$\bigcup_{\mathbf{t} \in \mathcal{T}} \left[\mathbf{t} + D^1 \cap \mathcal{M}^{00} \cap (\mathcal{M}^{00} - \mathbf{e}_1) \right], \tag{55}$$

which contains $\mathbb{Z}_n^2$ *if*

$$1 \leq \tau \leq \min\{m - 2, (m+1)/2\}. \tag{56}$$

Proof. For $\mathbf{n} \in D^1 \cap \mathcal{M}^{00} \cap (\mathcal{M}^{00} - \mathbf{e}_1)$, we have

$$h(\mathbf{n}+\mathbf{t}) = h(\mathbf{n}+\mathbf{e}_1) - \mathrm{i}\Delta^1 + \mathrm{i}\theta_{\mathbf{t}} - \mathrm{i}\theta_{00} \tag{57}$$

by (52) and (47).

Hence, by (47) and (57),

$$\begin{aligned} h(\mathbf{n}+\mathbf{e}_1+\mathbf{t}) &= h(\mathbf{n}+\mathbf{e}_1) + \mathrm{i}\theta_{\mathbf{t}} - \mathrm{i}\theta_{00} \\ &= h(\mathbf{n}+\mathbf{t}) + \mathrm{i}\Delta^1. \end{aligned}$$

In other words, (52) has been extended to $\mathbf{t} + D^1 \cap \mathcal{M}^{00} \cap (\mathcal{M}^{00} - \mathbf{e}_1)$. Taking the union over all shifts, we obtain (55).

For the second part of the proposition, let us write the set (55) explicitly as

$$\bigcup_{k,l=0}^{q-1} \{\mathbf{t}_{kl} + [([\![0, m-\tau-1]\!] \cup [\![\tau-1, m-1]\!]) \cap [\![0, m-2]\!]] \times [\![0, m-1]\!]\}$$

provided that $\tau \geq 1$. Note that

$$\begin{aligned} [([\![0, m-\tau-1]\!] \cup [\![\tau-1, m-1]\!]) \cap [\![0, m-2]\!]] &= [\![0, m-\tau-1]\!] \cup [\![\tau-1, m-2]\!] \\ &= [\![0, m-2]\!] \end{aligned}$$

under $m - \tau - 1 \geq \tau - 2$ or, equivalently, $\tau \leq (m+1)/2$. To complete the argument for the sufficient condition (56), observe that the adjacent rectangles among

$$(\tau(k,l) + (\delta_k^1, \delta_l^2) + [\![0, m-2]\!]) \times [\![0, m-1]\!], \quad k, l = 0, \ldots, q-1,$$

have zero gap if $\tau \leq m - 2$. ∎

By the same argument under (56), it follows from (49) that for all $\mathbf{n} \in \mathbb{Z}_n^2$

$$h(\mathbf{n}+(0,1)) = h(\mathbf{n}) + \mathrm{i}\Delta^2 \mod \mathrm{i}2\pi, \quad \Delta^2 := 2\mathrm{i}\theta_{01} - \mathrm{i}\theta_{02} - \mathrm{i}\theta_{00}. \tag{58}$$

In conclusion,

$$h(\mathbf{n}) = h(0) + \mathrm{i}\mathbf{n}\cdot\mathbf{r} \mod \mathrm{i}2\pi \quad \forall \mathbf{n} \in \mathbb{Z}_n^2, \tag{59}$$

where $\mathbf{r} = (\Delta^1, \Delta^2)$.

5.2. General perturbation. Next we consider more general perturbations $\{\delta_k^i\}$ to the raster scan and derive (59).

Let us rewrite (47) in a different form. Subtracting the respective (47) for $\mathbf{t}$ and $\mathbf{t}'$, we obtain the equivalent form

$$h(\mathbf{n}+\mathbf{t}) - h(\mathbf{n}+\mathbf{t}') = \mathrm{i}\theta_{\mathbf{t}} - \mathrm{i}\theta_{\mathbf{t}'} \mod \mathrm{i}2\pi \tag{60}$$

for any $\mathbf{n} \in \mathcal{M}^{00}$ and $\mathbf{t}, \mathbf{t}' \in \mathcal{T}$, which can also be written as

$$h(\mathbf{n}+\mathbf{t}-\mathbf{t}') = h(\mathbf{n}) + \mathrm{i}(\theta_{\mathbf{t}} - \theta_{\mathbf{t}'}) \mod \mathrm{i}2\pi \tag{61}$$

for $\mathbf{n} \in \mathcal{M}^{\mathbf{t}'}$ by shifting the argument of h.

Consider the triplets of shifts

$$(\mathbf{t}_{kl}, \mathbf{t}_{k+1,l}, \mathbf{t}_{k+2,l}), \quad (\mathbf{t}_{kl}, \mathbf{t}_{k,l+1}, \mathbf{t}_{k,l+2})$$

for which we have

$$2(\mathbf{t}_{k+1,l}-\mathbf{t}_{kl})-(\mathbf{t}_{k+2,l}-\mathbf{t}_{kl})=(2\delta^1_{k+1}-\delta^1_k-\delta^1_{k+2},0):=(a^1_k,0),$$
$$2(\mathbf{t}_{k,l+1}-\mathbf{t}_{kl})-(\mathbf{t}_{k,l+2}-\mathbf{t}_{kl})=(0,2\delta^2_{l+1}-\delta^2_l-\delta^2_{l+2}):=(0,a^2_l).$$

Analogous to (53) and (50) the paths of reduction

$$(2\mathbf{t}_{k+1,l}-\mathbf{t}_{kl}-\mathbf{t}_{k+2,l})\longrightarrow 2(\mathbf{t}_{k+1,l}-\mathbf{t}_{kl})\longrightarrow(\mathbf{t}_{k+1,l}-\mathbf{t}_{kl})\longrightarrow(0,0)$$

and

$$(2\mathbf{t}_{k+1,l}-\mathbf{t}_{kl}-\mathbf{t}_{k+2,l})\longrightarrow(\mathbf{t}_{k+1,l}-\mathbf{t}_{k+2,l})\longrightarrow(\mathbf{t}_{k+1,l}-\mathbf{t}_{kl})\longrightarrow(0,0)$$

lead to

$$h(\mathbf{n}+(a^1_k,0))=h(\mathbf{n})+2\mathrm{i}\theta_{k+1,l}-\mathrm{i}\theta_{k+2,l}-\mathrm{i}\theta_{kl}\mod \mathrm{i}2\pi \tag{62}$$

for all $\mathbf{n}\in D^1_{kl}$, where

$$\begin{aligned}D^1_{kl}:=&\left\{\mathcal{M}^{kl}\cap\left[\mathcal{M}^{kl}-2\mathbf{t}_{k+1,l}+\mathbf{t}_{k+2,l}+\mathbf{t}_{kl}\right]\cap\left[\mathcal{M}^{kl}-\mathbf{t}_{k+1,l}+\mathbf{t}_{kl}\right]\right\}\\&\bigcup\left\{\mathcal{M}^{kl}\cap\left[\mathcal{M}^{kl}+\mathbf{t}_{k+2,l}-\mathbf{t}_{k+1,l}\right]\right\}\\=&\left\{\mathcal{M}^{kl}\cap\left[\mathcal{M}^{kl}-(a^1_k,0)\right]\cap[\mathcal{M}^{kl}-(\tau+\delta^1_{k+1}-\delta^1_k,0)]\right\}\\&\bigcup\left\{\mathcal{M}^{kl}\cap\left[\mathcal{M}^{kl}+(\tau+\delta^1_{k+2}-\delta^1_{k+1},0)\right]\right\}\end{aligned}$$

Likewise, repeatedly applying (61) along the paths,

$$(2\mathbf{t}_{k,l+1}-\mathbf{t}_{kl}-\mathbf{t}_{k,l+2})\longrightarrow 2(\mathbf{t}_{k,l+1}-\mathbf{t}_{kl})\longrightarrow(\mathbf{t}_{k,l+1}-\mathbf{t}_{kl})\longrightarrow(0,0)$$

and

$$(2\mathbf{t}_{k,l+1}-\mathbf{t}_{kl}-\mathbf{t}_{k+2,l})\longrightarrow(\mathbf{t}_{k+1,l}-\mathbf{t}_{k+2,l})\longrightarrow(\mathbf{t}_{k+1,l}-\mathbf{t}_{kl})\longrightarrow(0,0),$$

we get

$$h(\mathbf{n}+(0,a^2_l))=h(\mathbf{n})+2\mathrm{i}\theta_{k,l+1}-\mathrm{i}\theta_{k,l+2}-\mathrm{i}\theta_{kl}\mod \mathrm{i}2\pi \tag{63}$$

for $\mathbf{n}\in D^2_{kl}$, where

$$\begin{aligned}D^2_{kl}:=&\left\{\mathcal{M}^{kl}\cap\left[\mathcal{M}^{kl}-2\mathbf{t}_{k,l+1}+\mathbf{t}_{k,l+2}+\mathbf{t}_{kl}\right]\cap\left[\mathcal{M}^{kl}-\mathbf{t}_{k,l+1}+\mathbf{t}_{kl}\right]\right\}\\&\bigcup\left\{\mathcal{M}^{kl}\cap\left[\mathcal{M}^{kl}+\mathbf{t}_{k,l+2}-\mathbf{t}_{k,l+1}\right]\right\}\\=&\left\{\mathcal{M}^{kl}\cap\left[\mathcal{M}^{kl}-(0,a^2_l)\right]\cap\left[\mathcal{M}^{kl}-(0,\tau+\delta^2_{l+1}-\delta^2_l)\right]\right\}\\&\bigcup\left\{\mathcal{M}^{kl}\cap\left[\mathcal{M}^{kl}+(0,\tau+\delta^2_{l+2}-\delta^2_{l+1})\right]\right\}.\end{aligned}$$

LEMMA 5.2. *Let k,l be fixed. Let $a^i_k=2\delta^i_{k+1}-\delta^i_k-\delta^i_{k+2}$, $i=1,2$. The relations* (62) *and* (63) *hold true in the sets*

$$\bigcup_{\mathbf{t}\in\mathcal{T}}\left[\mathbf{t}+D^1_{kl}\cap\mathcal{M}^{kl}\cap\left(\mathcal{M}^{kl}-\left(a^1_k,0\right)\right)\right] \tag{64}$$

and

$$\bigcup_{\mathbf{t}\in\mathcal{T}}\left[\mathbf{t}+D^2_{kl}\cap\mathcal{M}^{kl}\cap\left(\mathcal{M}^{kl}-\left(0,a^2_l\right)\right)\right], \tag{65}$$

respectively. Both sets contain $\mathbb{Z}_n^2$ *if the following conditions hold: for* $i = 1, 2$,

$$2\tau \le m - \max_{i=1,2} \left\{\delta^i_{k+2} - \delta^i_k\right\}, \tag{66}$$

$$\max_{i=1,2} \left[|a^i_k| + \max_{k'} \left\{\delta^i_{k'+1} - \delta^i_{k'}\right\}\right] \le m - \tau, \tag{67}$$

$$\delta^i_{k+1} - \delta^i_{k+2} \le \tau \le m - 1 + \delta^i_{k+1} - \delta^i_{k+2}. \tag{68}$$

Remark 5.3. Proposition 5.1 corresponds to $(k, l) = (0, 0)$ with (66), (67), and (68) reduced to

$$1 \le \tau \le (m + 1)/2.$$

Remark 5.4. Inequalities (68) and (67) are smallness conditions for the perturbations relative to the average step size and the overlap between the adjacent probes. The most consequential condition (66) suggests an average overlap ratio of at least 50%, i.e., undershifted raster scan.

Proof. The argument follows the same pattern as that for Proposition 5.1.

For $\mathbf{n} \in D^1_{kl} \cap \mathcal{M}^{00} \cap (\mathcal{M}^{00} - (a^1_k, 0))$, we have

$$h(\mathbf{n} + \mathbf{t}) = h(\mathbf{n} + (a^1_k, 0)) - \mathrm{i}(2\theta_{k+1,l} - \theta_{k+2,l} - \theta_{kl}) + \mathrm{i}\theta_{\mathbf{t}} - \mathrm{i}\theta_{00}$$

by (62) and (47).

Hence, by (47) and (57),

$$\begin{aligned} h\left(\mathbf{n} + \left(a^1_k, 0\right) + \mathbf{t}\right) &= h\left(\mathbf{n} + \left(a^1_k, 0\right)\right) + \mathrm{i}\theta_{\mathbf{t}} - \mathrm{i}\theta_{00} \\ &= h(\mathbf{n} + \mathbf{t}) + \mathrm{i}\left(2\theta_{k+1,l} - \theta_{k+2,l} - \theta_{kl}\right). \end{aligned}$$

Taking the union over all shifts, we obtain the set in (64). The case for (65) is similar.

For the second part of the proposition, note that

$$\begin{aligned} \mathcal{M}^{kl} \cap (\mathcal{M}^{kl} - (a^1_k, 0)) = \mathbf{t}_{kl} + [\![0, m - 1 - a^1_k]\!] \times [\![0, m - 1]\!] \quad \text{if} \quad a^1_k \ge 0 \\ \text{or } \mathbf{t}_{kl} + [\![-a^1_k, m - 1]\!] \times [\![0, m - 1]\!] \quad \text{if} \quad a^1_{kl} < 0. \end{aligned} \tag{69}$$

In the former case in (69) the set (64) contains

$$\begin{aligned} \bigcup_{\mathbf{t} \in \mathcal{T}} \big[\mathbf{t} + \mathbf{t}_{kl} + \big([\![0, m - 1 - \tau - \delta^1_{k+1} + \delta^1_k]\!] \cup [\![\tau + \delta^1_{k+2} - \delta^1_{k+1}, m - 1]\!]\big) \\ \times [\![0, m - 1]\!] \cap \big([\![0, m - 1 - a^1_k]\!] \times [\![0, m - 1]\!]\big)\big] \end{aligned} \tag{70}$$

under the condition

$$\delta^1_{k+1} - \delta^1_{k+2} \le \tau \le m - 1 + \delta^1_{k+1} - \delta^1_{k+2}. \tag{71}$$

Further, the set in (70) becomes

$$\begin{aligned} \bigcup_{\mathbf{t} \in \mathcal{T}} \big[\mathbf{t} + \mathbf{t}_{kl} + \big([\![0, m - 1]\!] \cap [\![0, m - 1 - a^1_k]\!]\big) \times [\![0, m - 1]\!]\big] \\ = \bigcup_{\mathbf{t} \in \mathcal{T}} \big[\mathbf{t} + \mathbf{t}_{kl} + [\![0, m - 1 - a^1_k]\!] \times [\![0, m - 1]\!]\big] \end{aligned} \tag{72}$$

under the condition

$$m - 1 - \tau - \delta^1_{k+1} + \delta^1_k \ge \tau + \delta^1_{k+2} - \delta^1_{k+1} - 1. \tag{73}$$

The set in (72) contains $\mathbb{Z}_n^2$ if for each l' the adjacent sets among

$$\mathbf{t}_{kl} + \tau(k', l') + \left(\delta_{k'}^1, \delta_{l'}^2\right) + [\![0, m - 1 - a_k^1]\!] \times [\![0, m - 1]\!],$$

for $k' = 0, \ldots, q - 1$, have no gap between them, which is the case if

$$\tau + \delta_{k'+1}^1 - \delta_{k'}^1 \leq m - |a_k^1| \quad \forall k'. \tag{74}$$

Likewise for the latter case in (69) the set in (64) contains

$$\bigcup_{\mathbf{t} \in \mathcal{T}} \big[\mathbf{t} + \mathbf{t}_{kl} + ([\![-a_k^1, m - 1 - \tau - \delta_{k+1}^1 + \delta_k^1]\!] \cup [\![\tau + \delta_{k+2}^1 - \delta_{k+1}^1, m - 1]\!]) \times [\![0, m - 1]\!] \cap \left([\![-a_k^1, m - 1]\!] \times [\![0, m - 1]\!]\right)\big] \tag{75}$$

under (71). The set in (75) in turn becomes

$$\bigcup_{\mathbf{t} \in \mathcal{T}} \left[\mathbf{t} + \mathbf{t}_{kl} + [\![-a_k^1, m - 1]\!] \times [\![0, m - 1]\!]\right]$$

under the condition (73). The set in (76) contains $\mathbb{Z}_n^2$ if for each l' the adjacent sets among

$$\mathbf{t}_{kl} + \tau(k', l') + \left(\delta_{k'}^1, \delta_{l'}^2\right) + [\![-a_k^1, m - 1]\!] \times [\![0, m - 1]\!],$$

for $k' = 0, \ldots, q - 1$, have no gap between them, which is the case under the same condition (74). Reorganizing the conditions (71), (73), and (74), we have (68), (66), and (67) with $i = 1$.

The case with (65) can be proved by exactly the same argument as above. ∎

Since $\mathcal{M}^{kl}$ overlaps with $\mathcal{M}^{k+1,l}$ and $\mathcal{M}^{k,l+1}$, which in turn overlap with $\mathcal{M}^{k+2,l}$ and $\mathcal{M}^{k,l+2}$, respectively (and so on), the quantities

$$\Delta_k^1 := 2\theta_{k+1,l} - \theta_{k+2,l} - \theta_{kl}, \tag{76}$$

$$\Delta_l^2 := 2\theta_{k,l+1} - \theta_{k,l+2} - \theta_{kl} \tag{77}$$

on the right-hand side of (62) and (63) depend only on one index.

Suppose further that there exist $c_k^1, c_l^2 \in \mathbb{Z}$ such that

$$\sum_{k=0}^{q-1} c_k^1 a_k^1 = \sum_{l=0}^{q-1} c_l^2 a_l^2 = 1, \tag{78}$$

i.e., $\{a_i^j\}$ are co-prime integers for each $j = 1, 2$.

Then by repeatedly using (62)–(63) we arrive at

$$h(\mathbf{n} + (1, 0)) = h\left(\mathbf{n} + \left(\sum_k c_k^1 a_k^1, 0\right)\right) = h(\mathbf{n}) + \mathrm{i}r_1 \mod \mathrm{i}2\pi,$$

$$h(\mathbf{n} + (0, 1)) = h\left(\mathbf{n} + \left(0, \sum_l c_l^2 a_l^2\right)\right) = h(\mathbf{n}) + \mathrm{i}r_2 \mod \mathrm{i}2\pi,$$

where

$$r_1 = \sum_{k=0}^{q-1} c_k^1 \Delta_k^1, \quad r_2 = \sum_{l=0}^{q-1} c_l^2 \Delta_l^2. \tag{79}$$

Therefore, we obtain (59) with $\mathbf{r} = (r_1, r_2)$ given by (79). Following through the rest of the argument we can prove the following result.

THEOREM 5.5. *Suppose that f does not vanish in $\mathbb{Z}_n^2$. For the perturbed raster scan* (41)*, let $\{\delta^i_{j_k}\}$ be the subset of perturbations satisfying*

$$2\tau \le m - \max_{i=1,2}\{\delta^i_{j_k+2} - \delta^i_{j_k}\}, \tag{80}$$

$$\max_{i=1,2}\left[|a^i_{j_k}| + \max_{k'}\{\delta^i_{k'+1} - \delta^i_{k'}\}\right] \le m - \tau, \tag{81}$$

$$\delta^i_{j_k+1} - \delta^i_{j_k+2} \le \tau \le m - 1 + \delta^i_{j_k+1} - \delta^i_{j_k+2}, \tag{82}$$

where $a^i_j = 2\delta^i_{j+1} - \delta^i_j - \delta^i_{j+2}, i = 1, 2$. Suppose

$$\gcd_{j_k}\left(|a^i_{j_k}|\right) = 1, \quad i = 1, 2. \tag{83}$$

Let $\mathbf{r} = (r_1, r_2) \in \mathbb{R}^2$ be given by (79) *and $\{c^j_i\}$ be any solution to* (78) *such that $\{c^i_{j_k}\}$ are the only nonzero entries.*

Then both the object and probe errors have a constant scaling factor and an affine phase profile:

$$g(\mathbf{n})/f(\mathbf{n}) = \alpha^{-1}(0)\exp(\mathrm{i}\mathbf{n}\cdot\mathbf{r}), \tag{84}$$

$$\nu^0(\mathbf{n})/\mu^0(\mathbf{n}) = \alpha(0)\exp(\mathrm{i}\phi(0) - \mathrm{i}\mathbf{n}\cdot\mathbf{r}). \tag{85}$$

Further the block phases have an affine profile:

$$\theta_{kl} = \theta_{00} + \mathbf{t}_{kl}\cdot\mathbf{r} \mod 2\pi \tag{86}$$

for $k, l = 0, \ldots, q-1$.

Remark 5.6. It can be verified through a tedious calculation that (86) (with (76)–(77), (78), and (79)) is an underdetermined linear system for $\{\theta_{kl}\}$, which is consistent with the fact that the affine phase ambiguity (1)–(2) is inherent to any blind ptychography.

Proof. It remains to verify (85) and (85), which follow immediately from (45) and (84).

The block phase relation (86) follows upon substituting $\mathbf{t} = \mathbf{t}_{kl}$ and (84) into (45).

To summarize, we have shown that the scaling factor in (85) and the affine phase ambiguity, in (84) and (85), are the only ambiguities for the slightly perturbed raster scan (41). ∎

6. Numerical experiments. In this section we demonstrate geometric convergence for blind ptychography with the perturbed raster scan (41).

Let $\mathcal{F}(\nu, g) \in \mathbb{C}^N$ be the totality of the Fourier (magnitude and phase) data corresponding to the probe ν and the object g such that $|\mathcal{F}(\mu, f)| = b$, where b is the noiseless ptychographic data. Since $\mathcal{F}(\cdot,\cdot)$ is a bilinear function, $A_k h := \mathcal{F}(\mu_k, h)$, $k \ge 1$, defines a matrix A_k for the kth probe estimate μ_k and $B_k\eta := \mathcal{F}(\eta, f_{k+1})$, $k \ge 1$, for the $(k+1)$st image estimate f_{k+1} such that $A_k f_{j+1} = B_j\mu_k$, $j \ge 1, k \ge 1$. Let $P_k = A_k A_k^\dagger$ be the orthogonal projection onto the range of A_k and $R_k = 2P_k - I$ the corresponding reflector. Likewise, let $Q_k = B_k B_k^\dagger$ be the orthogonal projection onto the range of B_k and S_k the corresponding reflector.

We use the amplitude-based objective function

$$\mathcal{L}(y) = \frac{1}{2}\||y| - b\|_2^2, \tag{87}$$

(a) f's real part (b) f's imaginary part (c) Randomly phased probe

FIG. 3. *The real part* (a) *and the imaginary part* (b) *of the object and* (c) *randomly phased probe* μ^{00} *where the color bar shows the probe phase in* $[-\pi, \pi]$.

which is nonconvex due to nonconvexity of phase retrieval (see [11] for discussion of other choices of objective functions). Blind ptychography is doubly nonconvex because, in addition to phase retrieval, extracting the probe and the object from the exit waves is also nonconvex.

For most nonconvex optimization, a good initialization is needed for convergence to the true solution (a global minimizer). For blind ptychography, however, we can at best hope for convergence to the true solution, up to the inherent ambiguities of a constant scaling factor and an affine phase factor. Worse still, all ptychographic solutions, including noninherent ambiguities, are global minimizers of $\mathcal{L}$ in (87). How is the algorithm going to distinguish a ptychographic solution from the true one?

In our simulation we initialize the probe estimate according to

$$|\phi - \phi_0| < \pi/2, \quad \phi(\mathbf{n}) = \arg\left[\mu_1(\mathbf{n})/\mu^{00}(\mathbf{n})\right] \quad \forall \mathbf{n} \in \mathcal{M}^{00} \tag{88}$$

for some arbitrary constant ϕ_0, where ϕ is well defined since μ^{00} vanishes nowhere. The choice of the initial probe amplitude $|\mu_1|$ is not essential. The constant phase factor ϕ_0 can be absorbed into the object estimate and set to zero. In other words, the probe guess gets the phase "roughly" right at every pixel. This, however, does not mean the initial probe is close to the true probe in any standard metric as, even with $|\mu_1(\mathbf{n})| = |\mu^{00}(\mathbf{n})| = \text{const.}$, the probe guess with uniformly distributed ϕ in $(-\pi/2, \pi/2]$ has the relative error (RE) close to

$$\sqrt{\frac{1}{\pi}\int_{-\pi/2}^{\pi/2} |e^{\mathrm{i}\phi} - 1|^2 d\phi} = \sqrt{2\left(1 - \frac{2}{\pi}\right)} \approx 0.8525$$

with high probability. Moreover, (88) allows many ambiguities given in Theorem 4.3 such as the periodic ($\mathbf{r} = 0$) ambiguities associated with arbitrary $|\psi| < \pi/2$ in (26) and (29).

As it stands, (88) represents certain prior information on the probe. In Algorithm 1, however, we enforce (88) only initially, but not in subsequent iterations.

The inner loops for updating the object and probe estimates are carried out by the Douglas–Rachford splitting method as detailed in [3, 11]: At epoch k, for $l = 1, 2, 3, \ldots,$

$$u_k^{l+1} = \frac{1}{2}u_k^l + \frac{1}{2}b \odot \operatorname{sgn}\big(R_k u_k^l\big), \quad u_k^1 = u_{k-1}^\infty, \tag{89}$$

$$v_k^{l+1} = \frac{1}{2}v_k^l + \frac{1}{2}b \odot \operatorname{sgn}\Big(S_k v_k^l\Big), \quad v_k^1 = v_{k-1}^\infty, \tag{90}$$

Algorithm 1. Alternating minimization

1: Input: initial probe guess μ_1.
2: Update the object estimate $f_{k+1} = \arg\min \mathcal{L}(A_k g)$ s.t. $g \in \mathbb{C}^{n\times n}$.
3: Update the probe estimate $\mu_{k+1} = \arg\min \mathcal{L}(B_k \nu)$ s.t. $\nu \in \mathbb{C}^{m\times m}$.
4: Terminate if $\mathcal{L}(B_k\mu_{k+1})$ stagnates or is less than tolerance; otherwise, go back to step 2 with $k \to k+1$.

with the object estimate $f_{k+1} = A_k^\dagger u_k^\infty$ and the probe estimate $\mu_{k+1} = B_k^\dagger v_k^\infty$, where u_k^∞ and v_k^∞ are terminal values of the kth epoch of the inner loops.

In the absence of additional prior information, any ptychographic solution, including all the ambiguities, is expected to be a fixed point of any iterative reconstruction. For Algorithm 1 with (89)–(90), this statement can be verified directly [11]. Since, as noted before, a significant portion of the periodic ambiguities in Theorem 4.3 are continuously distributed within the bound (88), the regular raster scan (with $\tau > 1$) would pose a great hinderance to reconstruction. Our numerical results with the irregular raster scans indicate that μ_1 under (88) falls in the basin of attraction of the true solution (up to the inherent ambiguities) in the sense of vanishing RE defined by

$$\mathrm{RE}(k) = \min_{\alpha\in\mathbb{C},\mathbf{k}\in\mathbb{R}^2} \frac{\|f(\mathbf{k}) - \alpha e^{-\imath 2\pi \mathbf{k}\cdot\mathbf{r}/n} f_k(\mathbf{k})\|_2}{\|f\|_2}, \tag{91}$$

where f_k is the recovered object at the kth epoch.

For efficiency, we keep the maximum number of iterations in the inner loop at 30 in our simulation.

The object is the 256-by-256 Cameraman+ i Barbara (CiB) (Figure 3(a), (b)). We use the randomly phased probe whose phases are 60×60 independent and identically distributed (i.i.d.) uniform random variables over $[0, 2\pi)$ (Figure 3(c)). The randomly perturbed raster scans (41) and (42) have the average step size $\tau = 30$ and perturbations δ_k^1 (resp., δ_{kl}^1) and δ_l^2 (resp., δ_{kl}^2) which are i.i.d. uniform random variables over $[\![-4, 4]\!]$. The average overlapping ratio $1 - \tau/m = 50\%$ is near the theoretical minimum.

When the probe steps outside of the boundary of the object domain, the margin $\bigcup_{kl} \mathcal{M}^{kl} \setminus \mathbb{Z}_n^2$ needs special treatment in the reconstruction process. We test five different boundary conditions. The periodic boundary condition forces the slope $\mathbf{r}$ in the linear phase ambiguity to be integer-valued. The dark-field and bright-field boundary conditions assume zero and nonzero (=100 in the simulation) values, respectively, in the margin. Depending our knowledge of the boundary condition, we may or may not enforce it.

Figure 4 shows RE over 100 epochs for the sampling schemes (41) and (42), with each curve corresponding to one run under a different boundary condition. In each case, (42) outperforms (41) with a faster convergence rate. This suggests that a higher level of disorder in the sampling scheme is better for ptychohgraphy (see also [3] and [11]). On the other hand, the regular raster scan (with $\tau > 1$) results in a non-vanishing RE (not shown) since the initialization condition (88) includes many other fixed points associated with the ambiguities given in Theorem 4.3.

For both perturbed schemes, the periodic boundary condition produces the fastest convergence, while the unenforced dark-field condition produces the slowest one. The constant bright-field boundary condition, when adopted and enforced, removes the affine phase ambiguity from the object estimate (i.e., $\mathbf{r} = 0$). Enforcing the dark-field

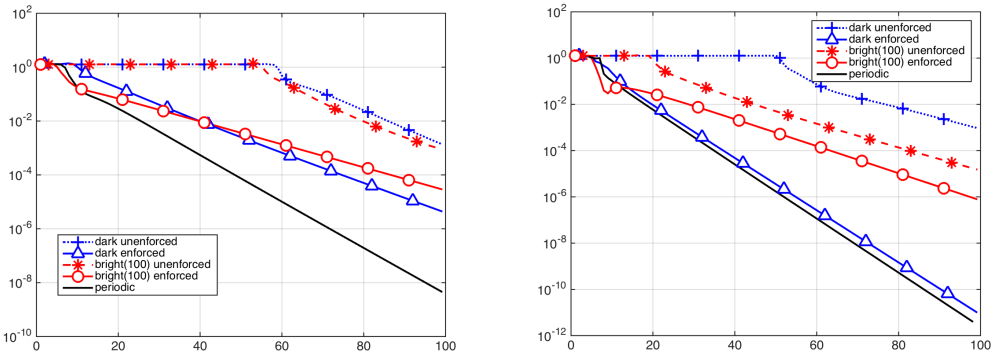

(a) RE vs. epoch with (41) (b) RE vs epoch with (42)

FIG. 4. *RE versus epoch for various boundary conditions with the sampling scheme* (a) (41) *and* (b) (42). *The difference in the vertical ranges in* (a) *and* (b) *indicates faster convergence with* (42).

boundary condition, however, does not remove the affine phase ambiguity. In both cases, enforcement of boundary condition speeds up the convergence.

7. Conclusion. We have studied the artifacts in blind ptychographic reconstruction from the perspective of uniqueness theory of inverse problems, in addition to the inherent ambiguities of a constant scaling factor and an affine phase factor. We have given a complete characterization of blind ptychographic ambiguities for the regular raster scan including the periodic and nonperiodic ambiguities.

The periodic ambiguities are the raster grid pathology reported in the optics literature, while the nonperiodic ambiguities have an affine profile varying on the intermediate scale of $\tau \times \tau$ block, instead of the fine scale of pixels as the affine phase factor. To the best of our knowledge, such an ambiguity has not been reported in the literature.

We have proved that a slightly perturbed undershifted raster scan can remove all the ambiguities except for those inherent to any blind ptychography. In comparison, the same goal is approached in [1] not by changing the raster scan but by restricting to a set of generic objects.

For the perturbed undershifted raster scan (41) with small random δ_j^i, it is highly probable that the co-prime condition (83) holds for large q and hence only the inherent ambiguities are present under (80)–(82) [19]. It would be interesting to see if the analysis presented in section 5 can be extended to other scan patterns in practice, such as the concentric circles [6, 36, 37], the Fermat spiral [13], and those designed for Fourier ptychography [13].

Empirically speaking, in a noisy ptychographic experiment with the raster scan, as the step size shrinks, raster grid pathology becomes less apparent and eventually invisible before the step size reaches 1 [14] (cf. Corollary 4.5). The affine phase ambiguity and the raster grid pathology can also be suppressed by additional prior information such as the Fourier intensities of the probe [23].

Acknowledgment. I thank the National Center for Theoretical Sciences (NCTS), Taiwan, where the present work was completed, for the hospitality during my visits in June and August 2018. I am grateful to Zheqing Zhang for preparing Figure 4.

REFERENCES

[1] T. Bendory, D. Edidin and Y. C. Eldar, *Blind Phaseless Short-Time Fourier Transform Recovery,* arXiv:1808.07414, 2018.

[2] O. Bunk, M. Dierolf, S. Kynde, I. Johnson, O. Marti, F. Pfeiffer, *Influence of the overlap parameter on the convergence of the ptychographical iterative engine,* Ultramicroscopy, 108 (2008), pp. 481–487.

[3] P. Chen and A. Fannjiang, *Coded-aperture ptychography: Uniqueness and reconstruction,* Inverse Problems, 34 (2018), 025003.

[4] H. H. Conway and N. J. A. Sloane, *Sphere Packings, Lattices and Groups*, 3rd ed., Springer-Verlag, Berlin, 1999.

[5] M. Dierolf, A. Menzel, P. Thibault, P. Schneider, C. M. Kewish, R. Wepf, O. Bunk, and F. Pfeiffer, *Ptychographic x-ray computed tomography at the nanoscale,* Nature, 467 (2010), pp. 436–439.

[6] M. Dierolf, P. Thibault, A. Menzel, C. Kewish, K. Jefimovs, I. Schlichting, K. Kong, O. Bunk, and F. Pfeiffer, *Ptychographic coherent diffractive imaging of weakly scattering specimens,* New J. Phys., 12 (2010), 035017.

[7] R. Egami, R. Horisaki, L. Tian, and J. Tanida, *Relaxation of mask design for single-shot phase imaging with a coded aperture,* Appl. Opt., 55 (2016), pp. 1830–1837.

[8] C. Falldorf, M. Agour, C. V. Kopylow, and R. B. Bergmann, *Phase retrieval by means of a spatial light modulator in the Fourier domain of an imaging system,* Appl. Opt., 49 (2010), pp. 1826–1830.

[9] A. Fannjiang and P. Chen, *Blind Ptychography: Uniqueness & Ambiguities,* arXiv:1806.02674, 2018.

[10] A. Fannjiang and W. Liao, *Phase retrieval with random phase illumination,* J. Opt. Soc. Am. A, 29, (2012), pp. 1847–1859.

[11] A. Fannjiang and Z. Zhang, *Blind Ptychography by Douglas-Rachford Splitting,* arXiv:1809.00962, 2018.

[12] M. Guizar-Sicairos, A. Diaz, M. Holler, M. S. Lucas, A. Menzel, R. A. Wepf, and O. Bunk, *Phase tomography from x-ray coherent diffractive imaging projections,* Opt. Express, 19 (2011), pp. 21345–21357.

[13] K. Guo, S. Dong, P. Nanda, and G. Zheng, *Optimization of sampling pattern and the design of Fourier ptychographic illuminator,* Opt. Express, 23 (2015), pp. 6171–6180.

[14] X. Huang, H. Yan, M. Ge, H. Öztörk, E. Nazaretski, I. K. Robinson, and Y. S. Chu, *Artifact mitigation of ptychography integrated with on-the-fly scanning probe microscopy,* Appl. Phys. Lett., 111 (2017), 023103.

[15] X. Huang, H. Yang, R. Harder, Y. Hwu, I.K. Robinson, and Y. S. Chu, *Optimization of overlap uniformness for ptychography,* Opt. Express, 22 (2014), pp. 12634–12644.

[16] R. Horisaki, R. Egami, and J. Tanida, *Single-shot phase imaging with randomized light (SPIRaL)*, Opt. Express, 24 (2016), pp. 3765–3773.

[17] M. A. Iwen, A. Viswanathan, and Y. Wang, *Fast phase retrieval from local correlation measurements,* SIAM J. Imaging Sci., 9 (2016), pp. 1655–1688.

[18] Y. Jiang, Z. Chen, Y. Han, P. Deb, H. Gao, S. Xie, P. Purohit, M. W. Tate, J. Park, S. M. Gruner, V. Elser, and D. A. Muller, *Electron ptychography of 2D materials to deep sub-angstrom resolution,* Nature, 559 (2018), pp. 343–349.

[19] A. M. Maiden, M. J. Humphry, F. Zhang, and J. M. Rodenburg, *Superresolution imaging via ptychography,* J. Opt. Soc. Am. A, 28 (2011), pp. 604–612.

[20] A. Maiden, D. Johnson, and P. Li, *Further improvements to the ptychographical iterative engine,* Optica, 4 (2017), pp. 736–745.

[21] A. M. Maiden, G. R. Morrison, B. Kaulich, A. Gianoncelli, and J. M. Rodenburg, *Soft X-ray spectromicroscopy using ptychography with randomly phased illumination,* Nat. Commun., 4 (2013), 1669.

[22] A. M. Maiden and J. M. Rodenburg, *An improved ptychographical phase retrieval algorithm for diffractive imaging,* Ultramicroscopy, 109 (2009), pp. 1256–1262.

[23] S. Marchesini, H. Krishnan, B. J. Daurer, D. A. Shapiro, T. Perciano, J. A. Sethian, and F. R. N. C. Maia, *SHARP: A distributed GPU-based ptychographic solver,* J. Appl. Cryst., 49 (2016), pp. 1245–1252.

[24] Y. S. G. Nashed, D. J. Vine, T. Peterka, J. Deng, R. Ross, and C. Jacobsen, *Parallel ptychographic reconstruction,* Opt. Express, 22 (2014), pp. 32082–32097.

[25] P. D. Nellist, B. C. McCallum, and J. M. Rodenburg, *Resolution beyond the information limit in transmission electron microscopy,* Nature, 374 (1995), pp. 630–632.

[26] P. D. Nellist and J. M. Rodenburg, *Electron ptychography.* I. *Experimental demonstration beyond the conventional resolution limits,* Acta Cryst. A, 54 (1998), pp. 49–60.
[27] K. A. Nugent, *Coherent methods in the X-ray sciences,* Adv. Phys., 59 (2010), pp. 1–99.
[28] X. Ou, G. Zheng, and C. Yang, *Embedded pupil function recovery for Fourier ptychographic microscopy,* Opt. Express, 22 (2014), pp. 4960–4972.
[29] X. Peng, G. J. Ruane, M. B. Quadrelli, and G. A. Swartzlander, *Randomized apertures: High resolution imaging in far field,* Opt. Express, 25 (2017), 296187.
[30] F. Pfeiffer, *X-ray ptychography,* Nat. Photon., 12 (2017), pp. 9–17.
[31] J. M. Rodenburg, *Ptychography and related diffractive imaging methods,* Adv. Imaging Electron Phys., 150 (2008), pp. 87–184.
[32] M. H. Seaberg, A. d'Aspremont, and J. J. Turner, *Coherent diffractive imaging using randomly coded masks,* Appl. Phys. Lett., 107 (2015), 231103.
[33] M. Stockmar, P. Cloetens, I. Zanette, B. Enders, M. Dierolf, F. Pfeiffer, and P. Thibault, *Near-field ptychography: Phase retrieval for inline holography using a structured illumination,* Sci. Rep., 3 (2013), 1927.
[34] D. Sylman, V. Micó, J. Garca, and Z. Zalevsky, *Random angular coding for superresolved imaging,* Appl. Opt., 49 (2010), pp. 4874–4882.
[35] P. Thibault, M. Dierolf, O. Bunk, A. Menzel, and F. Pfeiffer, *Probe retrieval in ptychographic coherent diffractive imaging,* Ultramicroscopy, 109 (2009), pp. 338–343.
[36] P. Thibault, M. Dierolf, A. Menzel, O. Bunk, C. David, F. Pfeiffer, *High-resolution scanning X-ray diffraction microscopy,* Science, 321 (2008), pp. 379–382.
[37] P. Thibault and A. Menzel, *Reconstructing state mixtures from diffraction measurements,* Nature, 494 (2013), pp. 68–71.
[38] F. Zhang, B. Chen, G. R. Morrison, J. Vila-Comamala, M. Guizar-Sicairos, and I. K. Robinson, *Phase retrieval by coherent modulation imaging,* Nat. Comm., 7 (2016), 13367.
[39] X. Zhang, J. Jiang, B. Xiangli, and G. R. Arce, *Spread spectrum phase modulation for coherent X-ray diffraction imaging,* Opt. Express, 23 (2015), pp. 25034–25047.
[40] G. Zheng, R. Horstmeyer, and C. Yang, *Wide-field, high-resolution Fourier ptychographic microscopy,* Nature Photonics, 7 (2013), pp. 739–745.